Monitoring of Singlet Oxygen Is Useful for Predicting the Photodynamic Effects in the Treatment for Experimental Glioma

Junkoh Yamamoto,[1] Seiji Yamamoto,[2] Toru Hirano,[2] Shaoyi Li,[1] Masayo Koide,[1] Eiji Kohno,[2] Mitsuo Okada,[1] Chikanori Inenaga,[1] Tsutomu Tokuyama,[1] Naoki Yokota,[1] Susumu Terakawa,[2] and Hiroki Namba[1]

Abstract

Purpose: Singlet oxygen ($^1O_2$) generated in photodynamic therapy (PDT) plays a very important role in killing tumor cells. Using a new near-IR photomultiplier tube system, we monitored the real-time production of $^1O_2$ during PDT and thus investigated the relationship between the $^1O_2$ production and photodynamic effects.

Experimental Design: We did PDT in 9L gliosarcoma cells *in vitro* and in an experimental tumor model *in vivo* using 5-aminolevulinic acid and nanosecond-pulsed dye laser. During this time, we monitored $^1O_2$ using this system. Moreover, based on the $^1O_2$ monitoring, we set the different conditions of laser exposure and investigated whether they could affect the tumor cell death.

Results: We could observe the temporal changes of $^1O_2$ production during PDT in detail. At a low fluence rate the $^1O_2$ signal gradually decreased with a low peak, whereas at a high fluence rate it decreased immediately with a high peak. Consequently, the cumulative $^1O_2$ at a low fluence rate was higher, which thus induced a strong photodynamic effect. The proportion of apoptosis to necrosis might therefore be dependent on the peak and duration of the $^1O_2$ signal. A low fluence rate tended to induce apoptotic change, whereas a high fluence rate tended to induce necrotic change.

Conclusions: The results of this study suggested that the monitoring of $^1O_2$ enables us to predict the photodynamic effect, allowing us to select the optimal laser conditions for each patient.

Photodynamic therapy (PDT) is very useful for several kinds of cancers, and many kinds of photosensitizers have thus far been established. Many researchers have tried to determine the optimal conditions in PDT. However, such attempts have all failed because it is extremely difficult to control and predict the photodynamic effect (1–3). PDT is done using a photosensitizer, which is selectively taken up and retained by neoplastic tissue. When activated by a laser with a proper wavelength, the photosensitizer causes direct cell death by generating reactive oxygen species that are cytotoxic. Especially, singlet oxygen ($^1O_2$) is supposed to play an important role (4, 5). If detecting $^1O_2$ is possible during PDT, we might thus be able to determine the optimal condition of each photosensitizer. Moreover, we may improve the photodynamic effects and elucidate the mechanisms of PDT. Some researchers have thus reported the methods for detecting $^1O_2$ generated by PDT and the correlations between the $^1O_2$ generation and efficacy of killing cells *in vitro*. However, few studies have thus far provided the data *in vivo* experimental tumor models to help determine the optimal conditions and to understand the mechanisms of cell death from the aspect of $^1O_2$ generation (6–9).

Generally, $^1O_2$ generated by PDT undergoes radiant decay, thus resulting in emission at 1,270-nm light (near-IR luminescence detection; ref. 10). For the detection of near-IR luminescence, a new near-IR photomultiplier tube (NIR-PMT) system (H9170-45, Hamamatsu Photonics K.K., Hamamatsu, Japan) has recently been developed and miniaturized for clinical application.

In this study, using the new NIR-PMT system, we investigated the possibility of real-time monitoring of $^1O_2$ generated by PDT in methylene blue solutions and in glioma cells *in vitro* and evaluated the tumor cell death caused by PDT. Thereafter, we measured $^1O_2$ in rat s.c. tumor model and evaluated the dependency of the antitumor effect of PDT on $^1O_2$ generation. We discussed its potency of using real-time monitoring of $^1O_2$ generated by PDT using the new NIR-PMT system.

Authors' Affiliations: [1]Department of Neurosurgery and [2]Photon Medical Research Center, Hamamatsu University School of Medicine, Hamamatsu, Japan
Received 3/31/06; revised 9/12/06; accepted 9/28/06.

Grant support: Japan Society for the Promotion of Science grant-in-aid for research fellow 15052531 (J. Yamamoto), Japan Society for the Promotion of Science grant 16390407 (S. Yamamoto), and Ministry of Education, Culture, Sports, Science and Technology, Japan, Center of Excellence grant-in-aid.

The costs of publication of this article were defrayed in part by the payment of page charges. This article must therefore be hereby marked *advertisement* in accordance with 18 U.S.C. Section 1734 solely to indicate this fact.

Requests for reprints: Seiji Yamamoto, Photon Medical Research Center, Hamamatsu University School of Medicine, 1-20-1 Handayama, Hamamatsu 431-3192, Japan. Phone: 81-53-435-2391; Fax: 81-53-435-2092; E-mail: seijiy@hama-med.ac.jp.

©2006 American Association for Cancer Research.

doi:10.1158/1078-0432.CCR-06-0786

Downloaded from clincancerres.aacrjournals.org on January 21, 2022. © 2006 American Association for Cancer Research.

Materials and Methods

Photosensitizer. Methylene blue was purchased from Sigma-Aldrich Japan K.K. (Tokyo, Japan), and it was dissolved in distilled water at a final concentration of 50 μmol/L in an *in vitro* study. 5-Aminolevulinic acid (5-ALA) was purchased from Cosmobio K.K. (Tokyo, Japan), and then it was dissolved in a fresh culture medium at a final concentration of 10 mmol/L in an *in vitro* study. In addition, 5-ALA was dissolved in PBS at a concentration of 100 mg/mL in an *in vivo* study. The pH of the solution was adjusted to 6.0 to 6.3 using a pH indicator paper by the addition of 1 N sodium hydroxide. The solution was used within 10 minutes after preparation. It was given i.v. to rats via the dorsal tail vein at a dose of 100 mg/kg body weight.

Antioxidants. L-Ascorbic acid was purchased from Sigma-Aldrich Japan K.K. (11). Catechin hydrate was purchased from Spectrum Chemical Manufacturing Corp. (Gardena, CA; refs. 12, 13), and these antioxidants were dissolved in distilled water at appropriate concentrations in an *in vitro* study. The structure of catechin is shown in Fig. 1E.

Laser source and light delivery system. A YAG-dye laser (Hamamatsu Photonics K.K.) was used in an *in vitro* and *in vivo* study. The laser was tuned to 665 nm for methylene blue–mediated PDT and to 635 nm for 5-ALA-induced protoporphyrin IX. The laser output during PDT was monitored with a power meter in every experiment. The maximum pulse energy was 4 mJ and its duration was 5 nanoseconds. The pulses were delivered at a rate of 30 Hz. A single quarts fiber interfaced to the laser was used to deliver light for the *in vitro* study. In the *in vivo* study, it was used with distal diffuser (length, 10 mm) for intratumoral irradiation.

Monitoring system. A new NIR-PMT system (H9170-45) and a schematic of experimental setup are shown in Fig. 1. The NIR light was collected from a sample using an optical fiber bundle (outer diameter, 3.5 mm), including 200 fibers (outer diameter, 240 μm), perpendicularly to the excitation laser light. Long-pass uncoated silicon filter (1,000 nm) was mounted in front of a condenser lens to block out the excitation light and minimize the fluorescence generated by the collection optics. Next, 1,270-nm luminescence, which originated from $^1O_2$ through the interfered filter, was collected into the PMT. The photon counts were integrated every 1 second for methylene blue–mediated PDT and every 10 and 15 seconds for 5-ALA-induced protoporphyrin IX for the *in vitro* and *in vivo* studies, respectively.

Brain tumor cell lines and animals. 9L gliosarcoma cells were cultured for several days in RPMI 1640 with 10% FCS at 37°C before use. Male Fisher 344 rats (9 weeks) purchased from SLC, Inc. (Hamamatsu, Japan) were used for the inoculation of 9L gliosarcoma cells. All following experiments were done according to the roles of animal experimentation and the guide for the care and use of laboratory animals of Hamamatsu University School of Medicine.

***Monitoring of $^1O_2$ production in methylene blue solutions* in vitro.** Methylene blue solutions (final concentration, 50 μmol/L) were held in quartz cuvettes (1 × 1 × 4 cm) and exposed to laser light (665 nm, 40 mW) from the outside of the cuvette. The samples were measured using this system for 20 seconds during irradiation. Distilled water was also similarly measured as a control. Next, to investigate whether the 1,270-nm luminescence originated from $^1O_2$ is quenchable, antioxidants were added to methylene blue solutions at a final concentration of 2 μmol/L to 3 mmol/L and $^1O_2$ was measured for 10 seconds while being immediately exposed to laser light. Methylene blue solutions without antioxidants were also similarly measured as a control. The photon counts for 10 seconds were added, and the results were shown as a percentage of the control. The top of cuvettes was open so that the samples were exposed to room air, and the light source-sample-detector geometry was kept constant throughout the experiments.

***Monitoring of $^1O_2$ production in 9L gliosarcoma cells* in vitro.** 9L gliosarcoma cells were incubated with complete medium containing 10 mmol/L 5-ALA for 4 hours. The cells were washed with PBS and then

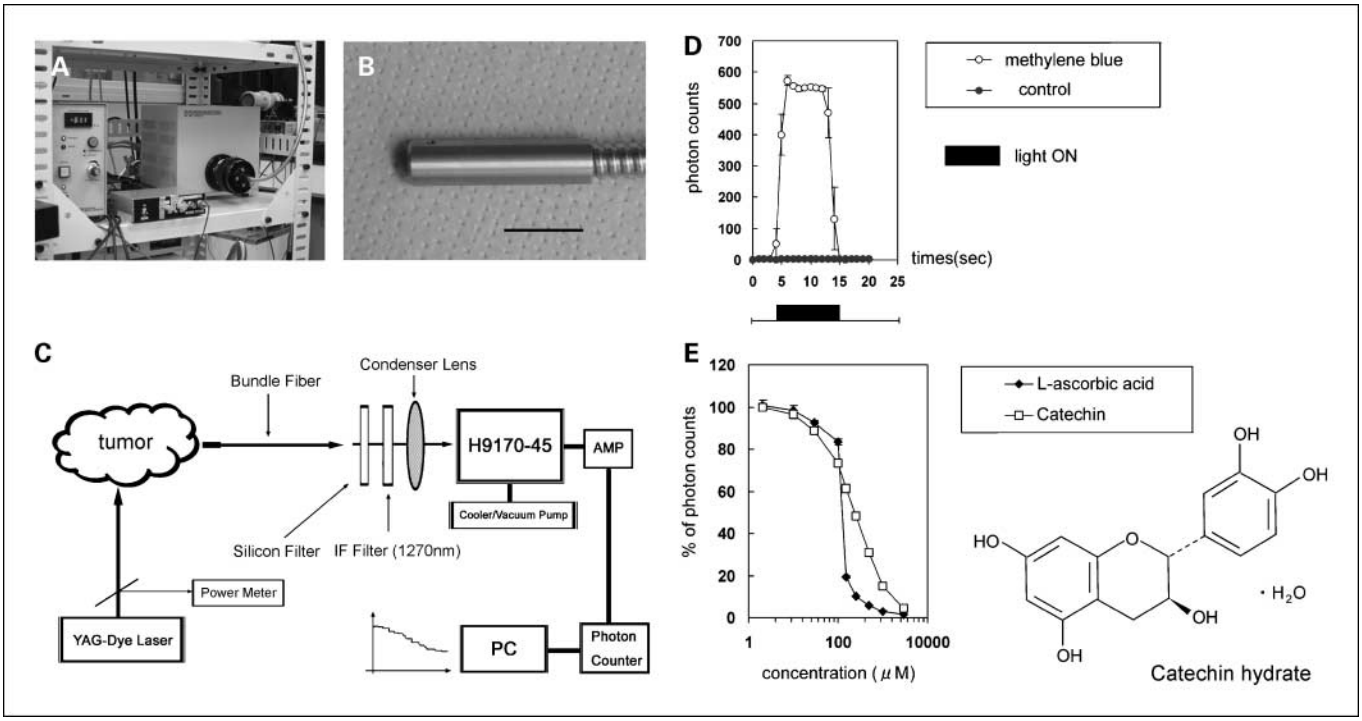

Fig. 1. *A,* the newly developed NIR-PMT system. *B,* tip of optical bundle fiber. Bar, 1 cm. *C,* schematic drawing of the experimental setup for *in vitro* and *in vivo* studies. *D,* temporal changes in the $^1O_2$ production in methylene blue. $^1O_2$ was generated by light exposure in methylene blue solutions. There was no signal in the control (water). *E,* quenching activity of the antioxidants in methylene blue solutions and chemical structure of catechin hydrate. Data were percentage of the control without any antioxidants. They were dependent on the concentrations of antioxidants. Points, mean; bars, SE.

Downloaded from clincancerres.aacrjournals.org on January 21, 2022. © 2006 American Association for Cancer Research.

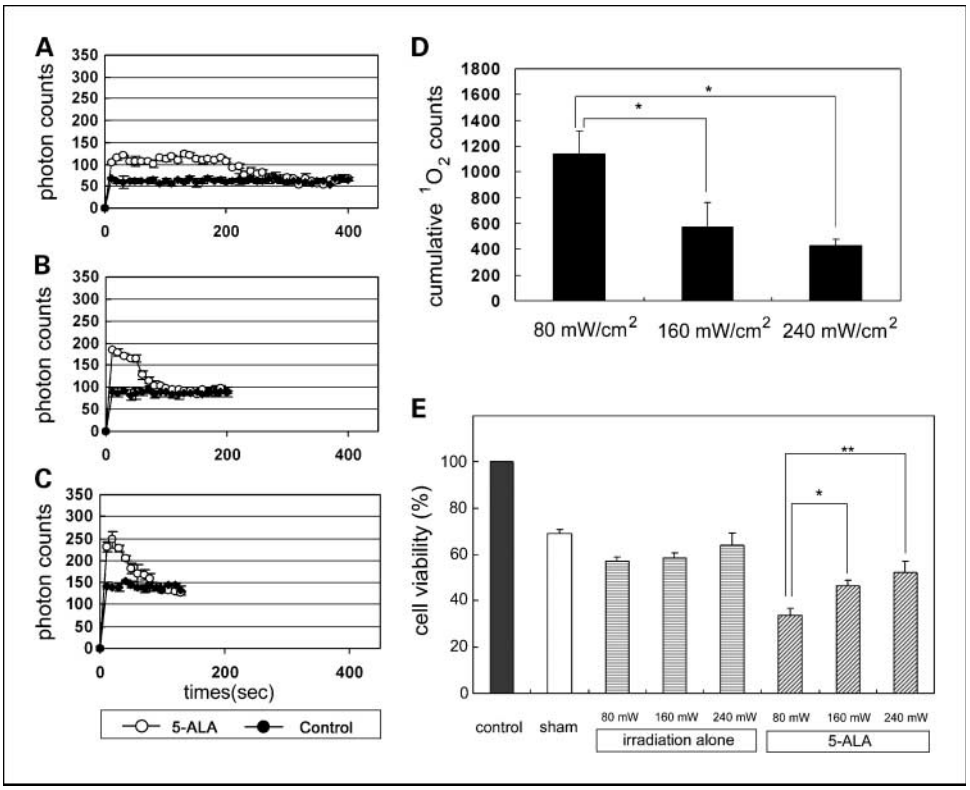

Fig. 2. Temporal changes of $^1O_2$ production in 9L cells during PDT. 9L cells were incubated with 5-ALA (10 mmol/L) for 4 hours and exposed by laser light (n = 3). The control was incubated without 5-ALA (n = 3). Total fluence was 32 J/cm^2. *A,* 80 mW/cm^2 (400 seconds). *B,* 160 mW/cm^2 (200 seconds). *C,* 240 mW/cm^2 (133 seconds). *D,* cumulative $^1O_2$ counts during PDT at each fluence rate. *E,* cell viability evaluated by MTT assay. The control group and the sham group were incubated with neither 5-ALA nor light exposure. However, the sham group was handled as the irradiation alone group was done but without any irradiation. Irradiation alone group was exposed by laser light without 5-ALA treatment (control in *A-C*). Note that irradiation alone did not show any effects compared with the sham group. Data were percentage of the control value. Columns, mean; bars, SE. *, $P < 0.05$; **, $P < 0.01$.

were detached with 0.5% trypsin solution. They were centrifuged and the pellets were thereafter resuspended in fresh medium. The samples were immediately transferred to the cuvette at concentration of 2.5 × 10^7 cells/mL in a 2.5-mL volume, and $^1O_2$ production was measured during PDT. The samples were irradiated at 80 mW/cm^2 (400 seconds), 160 mW/cm^2 (200 seconds), and 240 mW/cm^2 (133 seconds; n = 3). Total fluence was 32 J/cm^2 at each group. The control cells were incubated without exposure to 5-ALA and irradiated similarly (n = 3). The cumulative $^1O_2$ counts were calculated after subtracting them from control counts at the same irradiance in each group.

After PDT, each sample was collected immediately. Tumor cells (1 × 10^4 per well) were seeded in 96-well plates and incubated with fresh medium. The cell viability was determined using the 3-(4,5-dimethylthiazol-2-yl)-2,5-diphenyltetrazolium bromide (MTT) assay at 24 hours after PDT (14). All samples were evaluated and the results were shown as the percentage of the dark control without exposure to 5-ALA.

Evaluation of tumor cell death by Annexin V-FITC and propidium iodide staining. 9L gliosarcoma cells (2 × 10^4 per dish) were seeded in culture dishes (Iwaki 35 mm/glass base dish, Asahi Techno Glass Co., Tokyo, Japan) and incubated with complete medium containing 10 mmol/L 5-ALA for 4 hours. The cells were washed with PBS and replaced in fresh medium. They were then exposed to laser light at 80 mW/cm^2 (100 seconds, 8 J/cm^2), 80 mW/cm^2 (200 seconds, 16 J/cm^2), and 240 mW/cm^2 (100 seconds, 24 J/cm^2) from the base of the culture plate (n = 3). The control cells were similarly incubated with 10 mmol/L 5-ALA medium but without light exposure (n = 3). The induction of apoptosis

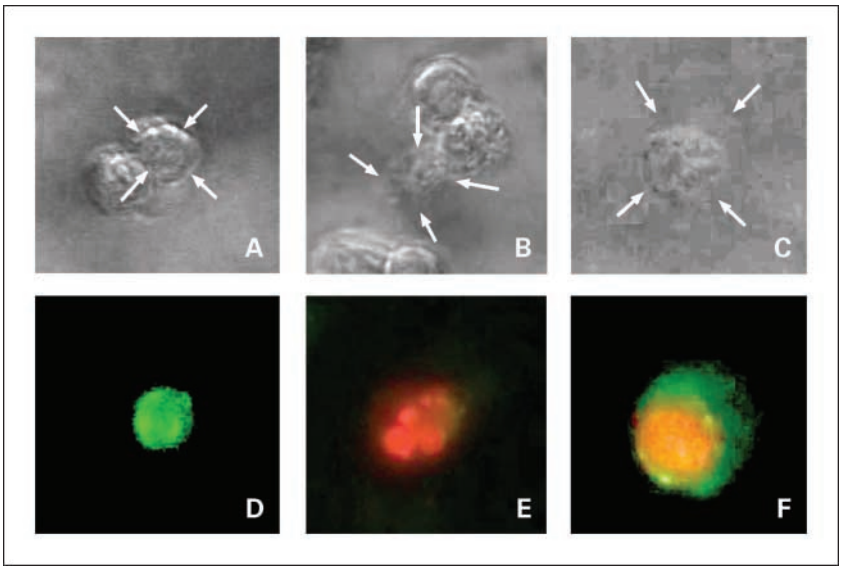

Fig. 3. Representative images by using Annexin V-FITC and propidium iodide staining in 9L cells *in vitro*. *A* to *C,* DIC images corresponded to the fluorescence images (*D-F*) of Annexin V-FITC and propidium iodide staining, respectively. The types of cell death were analyzed using the microscopic images (fluorescence and DIC images). *A* and *D,* early apoptotic cell. Note that the cell without swelling was FITC positive and propidium iodide negative. *B* and *E,* late apoptotic cell. Note that the cell with fragmentated nucleus was propidium iodide positive. *C* and *F,* necrotic cell. Note that the swollen cell was FITC and propidium iodide positive. *A* and *C,* arrows, cells insulted by PDT.

Downloaded from clincancerres.aacrjournals.org on January 21, 2022. © 2006 American Association for Cancer Research.

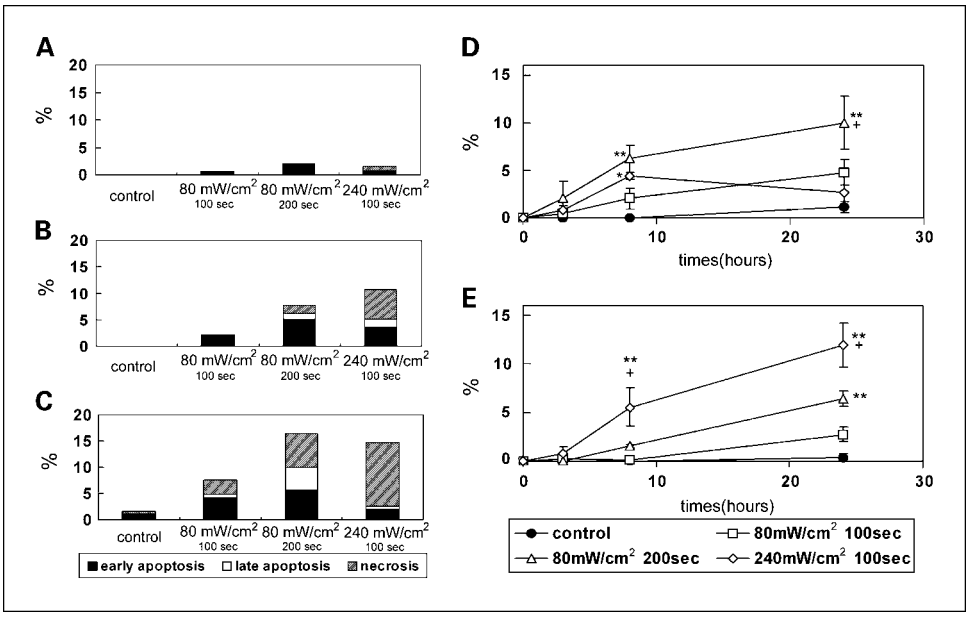

Fig. 4. Proportion of cell death after PDT under different laser conditions. The control was incubated with 5-ALA but without light exposure. *A,* 3 hours after PDT. *B,* 8 hours after PDT. *C,* 24 hours after PDT. *D,* temporal process of apoptotic cells (early and late apoptosis) replotted from (*A-C*). *, $P < 0.05$ versus control; **, $P < 0.01$ versus control; +, $P < 0.05$ versus 240 mW/cm^2 (100 seconds). *E,* temporal process of necrotic cells replotted from (*A-C*). **, $P < 0.01$ versus control; +, $P < 0.05$ versus 80 mW/cm^2 (200 seconds). Points, mean; bars, SE.

and necrosis was examined by the Annexin V-FITC and propidium iodide (Molecular Probes, Inc., Eugene, OR) staining (15). At 3, 8, and 24 hours after PDT, the tumor cells were rinsed gently and stained with PBS-containing Annexin V-FITC plus propidium iodide (10 μmol/L) in the dark at room temperature for 30 minutes. The tumor cells were then observed under a differential interference contrast (DIC) microscope (Axiovert 10, Zeiss, Oberkochen, Germany) with a 40× DIC objective lens and fluorescence optics [excitation at 488 nm, >515 nm emission for Annexin V-FITC (green) and for propidium iodide (red)]. The DIC image of the tumors and the fluorescence image of Annexin V-FITC and propidium iodide staining were obtained with a color-chilled three-chip charge-coupled device camera (C5810, Hamamatsu Photonics K.K.). This method can discriminate between late apoptosis and necrosis because we observe directly the images of tumor cells (16). Therefore, it is basically different from flow cytometric analysis. We thus evaluated the morphologic differentiation of cell death by this fluorescence imaging. The percentages of early or late apoptosis and of necrosis were respectively calculated by counting the number of all tumor cells (in DIC mode) and that of the cell stained with Annexin V-FITC and propidium iodide (in the fluorescence mode). Under the microscope, three fields were chosen at random in each dish.

Monitoring of the $^1O_2$ production in a rat s.c. tumor model. 9L gliosarcoma cells (1×10^6) were implanted in the dorsal skin of Fisher 344 rats. At 13 days after tumor implantation, under the anesthesia, intratumoral irradiation of the s.c. tumors was done at 30 mW/cm (900 seconds), 60 mW/cm (450 seconds), and 120 mW/cm (225 seconds) 4 hours after the i.v. administration of 5-ALA (100 mg/kg; $n = 6$). Total fluence was 27 J/cm at each group. The control groups were given without 5-ALA and irradiated at each fluence similarly ($n = 3$). According to our method of interstitial PDT (9), briefly, an optical fiber was inserted through the laser-proof colorless and transparent sheath of the 14-gauge needle and tip was placed in the center of the tumor for the efficient delivery of the light. After the hair covering the skin was removed, the detector was placed on the skin of the tumor perpendicular to the optical fiber. The $^1O_2$ production during PDT was monitored in all animals. The cumulative $^1O_2$ counts were calculated after subtraction with control counts at the same irradiance in each group.

Thereafter, all animals were sacrificed at 48 hours after PDT under the deep anesthesia. The tumor tissue specimens were removed immediately and then were cut perpendicular to the optical fiber track at the center of the tumor. The one side of the section was stained with 2,3,5-triphenyltetrazolium chloride (TTC) and scanned with a color scanner (9, 17). The area of tumor tissues damaged by PDT was calculated using an image processing software program (Scion Image, Scion Corporation, Frederick, MD), and the results were shown as the percentage of the total cross section of each tissue. The other side of the section was fixed with 20% formaldehyde/PBS. Continuous sections of all specimens were prepared in 30 mW/cm group and 120 mW/cm group, respectively. They were stained with H&E and terminal deoxynucleotidyl transferase–mediated dUTP nick end labeling (TUNEL) assay (*In situ* Cell Death Detection kit, Roche Diagnostics, Basel, Switzerland). We defined the cell that was dyed with TUNEL and observed nuclear fragmentation morphologically as "TUNEL-positive cell" (apoptotic cell). The percentage of TUNEL-positive cell was calculated by counting all the tumor cells in TUNEL assay. Under the microscope, three fields, which numerous TUNEL-positive cells gathered, were chosen in each sample.

Statistical analyses. The data are presented as the mean ± SE and were analyzed with Fisher's protected least significant difference. Significance was defined as $P < 0.05$.

Results

In vitro *real-time monitoring of $^1O_2$ production in methylene blue solution.* This NIR-PMT system proved to be extremely sensitive for detecting 1,270-nm light (i.e., $^1O_2$ generated by PDT; Fig. 1D). Moreover, these signals were dramatically quenched by L-ascorbic acid and catechin. These antioxidants are reported as quencher for reactive oxygen species, such as $^1O_2$ (11–13). Although the quenching activities of these antioxidants varied, they showed dose-dependent effects (Fig. 1E). We therefore considered this system to be very suitable for monitoring the $^1O_2$ generation during PDT.

***Real-time monitoring of $^1O_2$ production during PDT in 9L cells* in vitro.** We could obviously detect the temporal changes of $^1O_2$ production during *in vitro* PDT using NIR-PMT system (Fig. 2A-C). The fluence rates varied in the peak and decay of $^1O_2$ signal. In the low fluence rate the $^1O_2$ signal decreased gradually with a low peak (Fig. 2A), whereas in the high fluence rate it decreased immediately with a high peak (Fig. 2C). Consequently, under a fixed fluence, the cumulative $^1O_2$ production increased as the fluence rate decreased (Fig. 2D).

Downloaded from clincancerres.aacrjournals.org on January 21, 2022. © 2006 American Association for Cancer Research.

The statistical differences between 80 mW/cm^2 and the other groups were significant. The 1,270-nm luminescence in the control groups (i.e., with vehicle alone) also increased as the fluence rate increased (Fig. 2A-C). However, they did not decay and were lower than that with 5-ALA in each group. These signals might contain autofluorescence, thus including the $^1O_2$ signal from endogenous porphyrin, and artificial noise. We therefore considered the value after subtracting from control counts to be the true $^1O_2$ signal generated by PDT.

The cell viability revealed statistical differences between the 5-ALA-treated group and the irradiation alone group at the same irradiance (Fig. 2E). Although no significant differences were observed among the samples in the irradiation alone group, the differences between 80 mW/cm^2 and the other samples were statistically significant in the 5-ALA-treated group. We also observed that there were no statistical differences between the control cells and the 5-ALA-treated cells without the irradiation (data not shown).

Evaluation of tumor cell death after PDT by Annexin V-FITC and propidium iodide staining. We could easily distinguish tumor cell death by fluorescence imaging by using Annexin V-FITC and propidium iodide staining (Fig. 3). The cell death

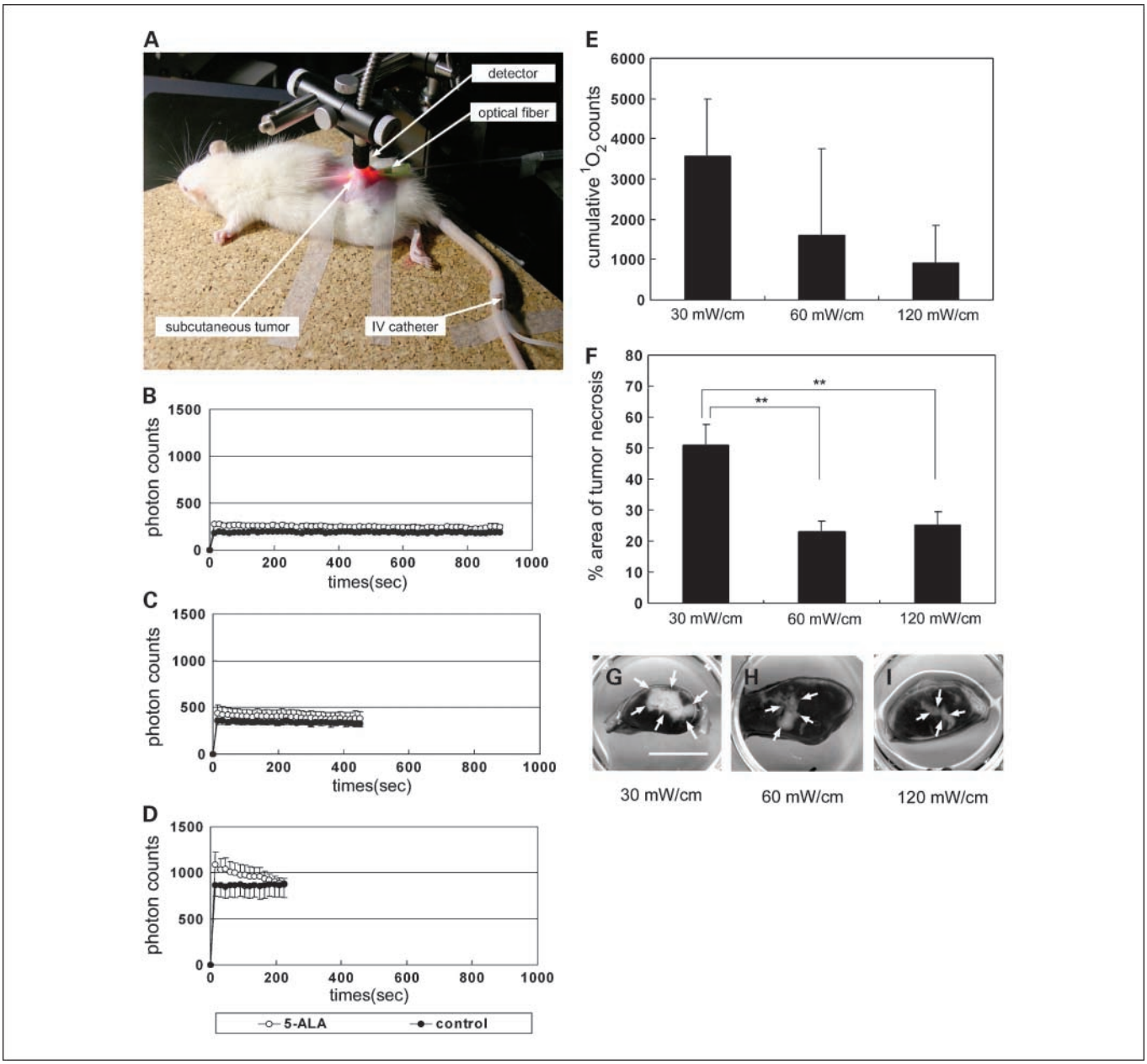

Fig. 5. *A,* an experimental setup used for monitoring of $^1O_2$ *in vivo*. *B* to *D,* temporal changes in the $^1O_2$ production during PDT. Intratumoral irradiation was done after 4 hours of i.v. administration of 5-ALA (100 mg/kg; $n = 6$). The control rats were exposed by laser light similarly without 5-ALA ($n = 3$). The total fluence was 27 J/cm. *B,* 30 mW/cm (900 seconds). *C,* 60 mW/cm (450 seconds). *D,* 120 mW/cm (225 seconds). *E,* cumulative $^1O_2$ production during PDT in 5-ALA-treated group. *F,* photodynamic effect evaluated by TTC stain. Data were percentage of the total cross sections in each tissue. Columns, mean; bars, SE. **, $P < 0.01$. Representative TTC-stained sections of a s.c. tumor in the 5-ALA-treated group. *G,* 30 mW/cm. *H,* 60 mW/cm. *I,* 120 mW/cm. Arrows, area of tumor damage. Bar, 1 cm.

Downloaded from clincancerres.aacrjournals.org on January 21, 2022. © 2006 American Association for Cancer Research.

occurred slowly after PDT in all groups, but the total number and the proportion varied (Fig. 4A-C). The majority of cell death in 80 mW/cm^2 (100 seconds) and 80 mW/cm^2 (200 seconds) showed early or late apoptosis in any time. In addition, both groups showed similar proportions of cell death. The total number of cell deaths in 80 mW/cm^2 (200 seconds) was about twice as many as that in 80 mW/cm^2 (100 seconds) at any time. On the other hand, the greater part of the cells in 240 mW/cm^2 resulted in necrosis. Despite the presence of a high fluence, the total number of cell deaths in 240 mW/cm^2 (100 seconds, 24 J/cm^2) was lower than that in 80 mW/cm^2 (200 seconds, 16 J/cm^2) at 3 and 24 hours after PDT.

Apoptotic (early and late) cells in 80 mW/cm^2 (200 seconds) significantly increased compared with the control group at 8 and 24 hours after PDT (Fig. 4D). In addition, the number of apoptotic cells in 80 mW/cm^2 (200 seconds) group was also significantly larger than those in 240 mW/cm^2 group at 24 hours ($P < 0.05$). Necrotic cells in 240 mW/cm^2 significantly increased compared with any other groups at 8 and 24 hours after PDT (Fig. 4E).

Monitoring of $^1O_2$ production in a rat s.c. tumor model. The tumor size (mean ± SD) before PDT was 11.3 ± 1.4 mm in length and 8.8 ± 1.4 mm in width. Our NIR-PMT system could clearly detect the change in $^1O_2$ production during PDT *in vivo* (Fig. 5A-D). At a low fluence rate, $^1O_2$ decreased gradually with a low peak, which was comparable with the results *in vitro*. On the other hand, a high fluence rate induced a high peak but rapidly decreased the $^1O_2$ production. There were no major differences in $^1O_2$ signals between control and 5-ALA-treated samples, especially at the fluence rate of 30 and 60 mW/cm. In the animal preparation *in vivo*, the light inside the body may show a lot of scattering and can produce noise detected by NIR-PMT system, inducing the large variation of the data. Although, due to the large variability in the *in vivo* study, the cumulative $^1O_2$ production did not reached the level of statistical differences between the control and 5-ALA-treated samples, they tended to decrease as the fluence rate increased (Fig. 5E), which was comparable with the results in the *in vitro* study.

Despite of the same rate of fluence, a difference in the fluence rate revealed different photodynamic effects in experimental tumors (Fig. 5F-I). The photodynamic effect in 30 mW/cm group was the strongest. On the other hand, those in 120 and 60 mW/cm were almost equivalent. In addition, no animals showed any systemic deterioration.

Histologic evaluation of s.c. 9L gliosarcomas after intratumoral PDT. The different types of cell death occurred obviously between 30 mW/cm group and 120 mW/cm group (Fig. 6A-C). Although each group showed the apoptotic changes in the boundary zones between the coagulation necrosis and the surviving tumor cells, the number of the apoptotic cells was more in 30 mW/cm group than in 120 mW/cm group. In addition, the TUNEL-positive cells in the former also significantly increased compared with the latter ($P < 0.01$; Fig. 6D). Although we also observed remarkable destruction of endothelial cells of tumor vessels, there were no differences that depend on the fluence rate (data not shown).

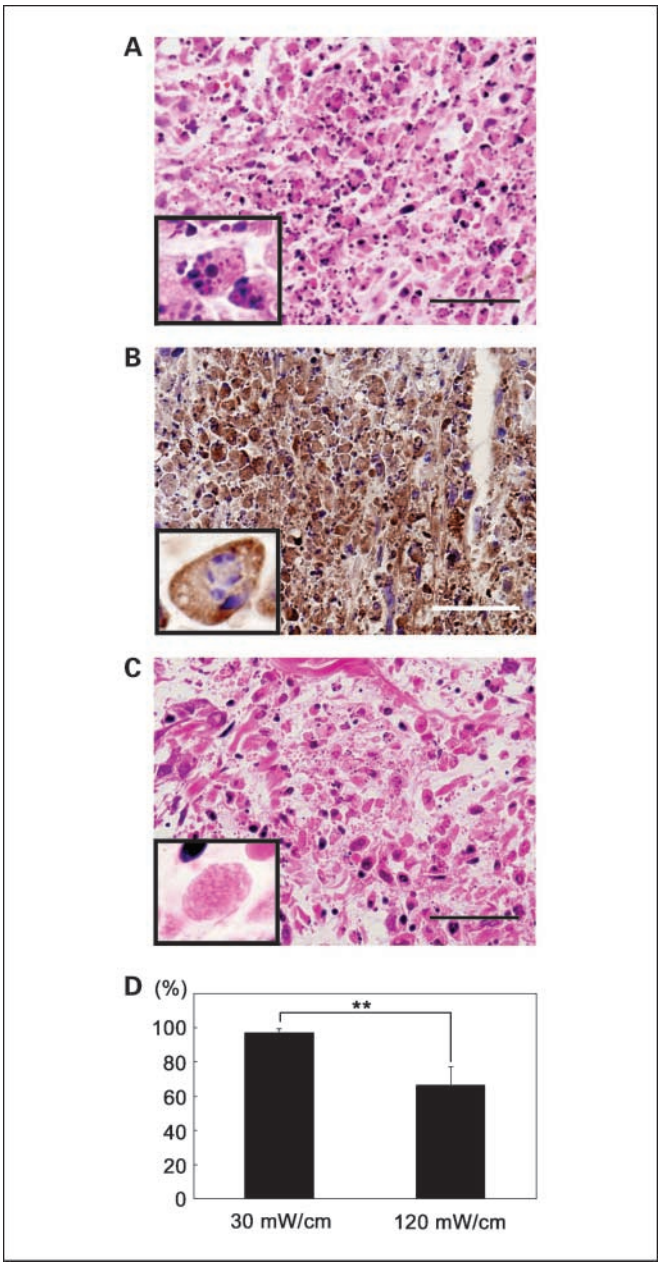

Fig. 6. Histologic evaluation of s.c. 9L gliosarcomas after PDT. *A* and *B*, H&E-stained section and the TUNEL assay in 30 mW/cm, respectively. *C*, H&E-stained section in 120 mW/cm. Magnified views of apoptotic cell (*A*), TUNEL-positive cell (*B*), and necrotic cell (*C*). Bar, 100 μm. *D*, percentages of TUNEL-positive cells. Columns, mean ($n = 6$); bars, SE. **, $P < 0.01$.

Discussion

In the present study, using experimental glioma, we measured in detail the temporal generation of $^1O_2$ during PDT and examined the photodynamic effects. We examined whether the condition of laser irradiation may affect the pattern of $^1O_2$ generation and whether the difference of $^1O_2$ generation could affect the photodynamic effects, including the types of cell death. We confirmed that irradiation with a low fluence rate generated a large amount of $^1O_2$ and induced strong photodynamic effects in agreement with another report (7).

Importance of monitoring $^1O_2$ for the optimal PDT. We have found that the different condition in laser irradiation varied $^1O_2$ production regarding the peak and decay of the $^1O_2$ signal. During PDT using 5-ALA, the irradiation with a low fluence rate

Downloaded from clincancerres.aacrjournals.org on January 21, 2022. © 2006 American Association for Cancer Research.

shows a long-lasting $^1O_2$ generation. To the contrary, a high fluence rate did not do so in agreement with another report (6). Although the mechanism of different effects between low and high fluence rates on $^1O_2$ production remains unclear at present, the possible explanations are as follows: (*a*) high fluence rate rapidly consumes and depletes intracellular oxygen (triplet oxygen; ref. 6), whereas low fluence rate allows to replenish the oxygen inside the cell; (*b*) high fluence rate may rapidly induce photobleaching (change in the formation of photosensitizer; refs. 18–20); and (*c*) the irradiance at high fluence rate gives excessive energy and transiently decreases the absorption of light in the photosensitizer (21). Irrespective of the mechanism, our results indicated that the optimal condition of irradiation should be decided based on the $^1O_2$ generation.

We also observed that $^1O_2$ was no longer generated once it reached the level of photobleaching,[3] indicating that the photo-induced degeneration of photosensitizer (photobleaching) is a terminal of irradiation. Moreover, the laser irradiation after photobleaching is excessive and may damage normal tissue (22–24). However, the duration of irradiation alone cannot predict the occurrence of photobleaching because the present study also showed that the fluence rate varied the duration that reached the photobleaching. Therefore, the generation of $^1O_2$ should be monitored during PDT. When we monitor the $^1O_2$ production using the detection system and adjust the laser fluence rate or laser pattern (continuous or intermittent) during PDT, it must allow us to do the appropriate PDT for each patients.

$^1O_2$ production deciding the type of tumor cell death in PDT. $^1O_2$ is produced under the photochemical reaction (type II), induces tumor cell death, and plays very important roles in PDT. In general, there are two types of cell death: one is necrosis and the other is apoptosis. The way in which cells die depends on the severity and the duration of insults that induce cell death. Many articles have reported that PDT induced either necrosis or apoptosis (9, 25–27). In fact, many complicated factors, including the kinds of photosensitizer, the types of tumor cells, the localization and the amount of photosensitizers, and the laser conditions (fluence and fluence rate), may determine the proportion of apoptosis and necrosis in PDT.

In our study using 9L cells and 5-ALA, the threshold may exist between 80 and 240 mW/cm^2 to determine the type of cell death. Low fluence rate (80 mW/cm^2) irradiance generates a low level of $^1O_2$ (Fig. 2A). This weak insult was below the threshold that can induce necrosis and then induced apoptosis. In addition, the incidence of apoptosis might depend on the periods of exposure below the threshold. The present study based on the monitoring of $^1O_2$ showed that the level of $^1O_2$ generation could decide not only the photodynamic effects but also the types of cell death. The results strongly suggested that $^1O_2$ plays a key mediator of the cell death during PDT.

Newly developed NIR-PMT system for detecting $^1O_2$ in clinical use. A further implication of this study should be considered. We propose the new NIR-PMT system, used in the present study, to be appropriate for detecting $^1O_2$ signals during PDT. Using this system, we showed that antioxidants quenched the $^1O_2$ signals and could monitor the $^1O_2$ production during PDT in an experimental tumor model and thus showed a relationship between the amounts of $^1O_2$ and photodynamic effects (Fig. 5).

Because the optimal laser condition may vary in the different photosensitizer, tumor type, and patient state, an indicator for optimal irradiation should be established during PDT. Some reports have proposed indicators for PDT by measuring the changes of temperature and oxygen consumption (28, 29). However, all of them were based on the indirect indicators. Although some methods of the direct detection of $^1O_2$, such as biochemical and electron spin resonance methods (30–32), have been reported, they cannot monitor the $^1O_2$ production during PDT of *in vivo* tumor and thus are unsuitable for clinical application. Our new system detects $^1O_2$ production through the optical fiber. Therefore, it can monitor the direct and focal production of $^1O_2$ during PDT *in vitro* and *in vivo*. This miniaturized, desktop-size system must be very useful in a clinical setting.

[3] Yamamoto J, Yamamoto S, Hirano T, Kohno E, unpublished data.

References

1. Goetz C, Hasan A, Stummer W, Heimann A, Kempski O. Experimental research photodynamic effects in perifocal, oedematous brain tissue. Acta Neurochir (Wien) 2002;144:173–9.
2. Kostron H, Obwegeser A, Jakober R. Photodynamic therapy in neurosurgery: a review. J Photochem Photobiol B 1996;36:157–68.
3. Kaye AH, Morstyn G, Apuzzo ML. Photoradiation therapy and its potential in the management of neurological tumors. J Neurosurg 1988;69:1–14.
4. Schweitzer C, Schmidt R. Physical mechanisms of generation and deactivation of singlet oxygen. Chem Rev 2003;103:1685–757.
5. Weishaupt KR, Gomer CJ, Dougherty TJ. Identification of singlet oxygen as the cytotoxic agent in photoinactivation of a murine tumor. Cancer Res 1976;36:2326–9.
6. Niedre MJ, Secord AJ, Patterson MS, Wilson BC. *In vitro* tests of the validity of singlet oxygen luminescence measurements as a dose metric in photodynamic therapy. Cancer Res 2003;63:7986–94.
7. Niedre MJ, Yu CS, Patterson MS, Wilson BC. Singlet oxygen luminescence as an *in vivo* photodynamic therapy dose metric: validation in normal mouse skin with topical amino-levulinic acid. Br J Cancer 2005;92:298–304.
8. Gorman AA, Rodgers MA. Current perspectives of singlet oxygen detection in biological environments. J Photochem Photobiol B 1992;14:159–76.
9. Yamamoto J, Hirano T, Li S, et al. Selective accumulation and strong photodynamic effects of a new photosensitizer, ATX-S10.Na (II), in experimental malignant glioma. Int J Oncol 2005;27:1207–13.
10. Krasnovsky AA, Jr. Singlet molecular oxygen in photobiochemical systems: IR phosphorescence studies. Membr Cell Biol 1998;12:665–90.
11. Hosaka S, Obuki M, Nakajima J, Suzuki M. Comparative study of antioxidants as quenchers or scavengers of reactive oxygen species based on quenching of MCLA-dependent chemiluminescence. Luminescence 2005;20:419–27.
12. Mukai K, Nagai S, Ohara K. Kinetic study of the quenching reaction of singlet oxygen by tea catechins in ethanol solution. Free Radic Biol Med 2005;39:752–61.
13. Guo Q, Zhao B, Shen S, et al. ESR study on the structure-antioxidant activity relationship of tea catechins and their epimers. Biochim Biophys Acta 1999;1427:13–23.
14. Mosmann T. Rapid colorimetric assay for cellular growth and survival: application to proliferation and cytotoxicity assays. J Immunol Methods 1983;65:55–63.
15. Koopman G, Reutelingsperger CP, Kuijten GA, et al. Annexin V for flow cytometric detection of phosphatidylserine expression on B cells undergoing apoptosis. Blood 1994;84:1415–20.
16. Matsumoto Y, Yamamoto S, Suzuki Y, et al. Na^+/H^+ exchanger inhibitor, SM-20220, is protective against excitotoxicity in cultured cortical neurons. Stroke 2004;35:185–90.
17. Bederson JB, Pitts LH, Germano SM, et al. Evaluation of 2,3,5-triphenyltetrazolium chloride as a stain for detection and quantification of experimental cerebral infarction in rats. Stroke 1986;17:1304–8.
18. Dysart JS, Singh G, Patterson MS. Calculation of singlet oxygen dose from photosensitizer fluorescence and photobleaching during mTHPC photodynamic therapy of MLL cells. Photochem Photobiol 2005;81:196–205.
19. Finlay JC, Mitra S, Patterson MS, Foster TH. Photobleaching kinetics of Photofrin *in vivo* and in

Downloaded from clincancerres.aacrjournals.org on January 21, 2022. © 2006 American Association for Cancer Research.

multicell tumour spheroids indicate two simultaneous bleaching mechanisms. Phys Med Biol 2004;49:4837–60.

20. Dysart JS, Patterson MS. Characterization of Photofrin photobleaching for singlet oxygen dose estimation during photodynamic therapy of MLL cells *in vitro*. Phys Med Biol 2005;50:2597–616.

21. Pogue BW, Momma T, Wu HC, Hasan T. Transient absorption changes *in vivo* during photodynamic therapy with pulsed-laser light. Br J Cancer 1999;80:344–51.

22. Chen Q, Chopp M, Madigan L, Dereski MO, Hetzel FW. Damage threshold of normal rat brain in photodynamic therapy. Photochem Photobiol 1996;64:163–7.

23. Ji Y, Walstad D, Brown JT, Powers SK. Interstitial photoradiation injury of normal brain. Lasers Surg Med 1992;12:425–31.

24. Powers SK, Cush SS, Walstad DL, Kwock L. Stereotactic intratumoral photodynamic therapy for recurrent malignant brain tumors. Neurosurgery 1991;29:688–95; discussion 95–6.

25. Luksiene Z, Eggen I, Moan J, Nesland JM, Peng Q. Evaluation of protoporphyrin IX production, phototoxicity, and cell death pathway induced by hexylester of 5-aminolevulinic acid in Reh and HPB-ALL cells. Cancer Lett 2001;169:33–9.

26. Bisland SK, Lilge L, Lin A, Rusnov R, Wilson BC. Metronomic photodynamic therapy as a new paradigm for photodynamic therapy: rationale and preclinical evaluation of technical feasibility for treating malignant brain tumors. Photochem Photobiol 2004;80:22–30.

27. Piette J, Volanti C, Vantieghem A, et al. Cell death and growth arrest in response to photodynamic therapy with membrane-bound photosensitizers. Biochem Pharmacol 2003;66:1651–9.

28. Wang HW, Putt ME, Emanuele MJ, et al. Treatment-induced changes in tumor oxygenation predict photodynamic therapy outcome. Cancer Res 2004;64:7553–61.

29. Gross S, Gilead A, Scherz A, Neeman M, Salomon Y. Monitoring photodynamic therapy of solid tumors online by BOLD-contrast MRI. Nat Med 2003;9:1327–31.

30. Atlante A, Passarella S. Detection of reactive oxygen species in primary cultures of cerebellar granule cells. Brain Res Protoc 1999;4:266–70.

31. Lavi R, Sinyakov M, Samuni A, et al. ESR detection of $^1O_2$ reveals enhanced redox activity in illuminated cell cultures. Free Radic Res 2004;38:893–902.

32. Wierrani F, Kubin A, Loew HG, et al. Photodynamic action of some sensitizers by photooxidation of luminol. Naturwissenschaften 2002;89:466–9.

Downloaded from clincancerres.aacrjournals.org on January 21, 2022. © 2006 American Association for Cancer Research.

AACR American Association for Cancer Research

Clinical Cancer Research

Monitoring of Singlet Oxygen Is Useful for Predicting the Photodynamic Effects in the Treatment for Experimental Glioma

Junkoh Yamamoto, Seiji Yamamoto, Toru Hirano, et al.

Clin Cancer Res 2006;12:7132-7139.

Updated version Access the most recent version of this article at:
http://clincancerres.aacrjournals.org/content/12/23/7132

Cited articles This article cites 32 articles, 6 of which you can access for free at:
http://clincancerres.aacrjournals.org/content/12/23/7132.full#ref-list-1

E-mail alerts Sign up to receive free email-alerts related to this article or journal.

Reprints and Subscriptions To order reprints of this article or to subscribe to the journal, contact the AACR Publications Department at pubs@aacr.org.

Permissions To request permission to re-use all or part of this article, use this link
http://clincancerres.aacrjournals.org/content/12/23/7132.
Click on "Request Permissions" which will take you to the Copyright Clearance Center's (CCC)
Rightslink site.

Downloaded from clincancerres.aacrjournals.org on January 21, 2022. © 2006 American Association for Cancer Research.